Global sensitivity analysis and uncertainties in SEA models of vibroacoustic systems

Jean-Loup Christen[a], Mohamed Ichchou[a], Bernard Troclet[b,c], Olivier Bareille[a], Morvan Ouisse[d]

[a] *École Centrale de Lyon, Université de Lyon, 36 avenue Guy de Collongue, 69130 Écully, France*
[b] *Airbus Defence and Space, 66 Route de Verneuil, 78133 Les Mureaux Cedex, France*
[c] *LMT, ENS Cachan, Université Paris-Saclay, 61 Avenue du Président Wilson, 94230 Cachan*
[d] *FEMTO-ST Applied Mechanics, ENSMM / UBFC, UMR CNRS 6174, 24 chemin de l'Épitaphe, 25000 Besançon*

Abstract

The effect of parametric uncertainties on the dispersion of Statistical Energy Analysis (SEA) models of structural-acoustic coupled systems is studied with the Fourier analysis sensitivity test (FAST) method. The method is firstly applied to an academic example representing a transmission suite, then to a more complex industrial structure from the space industry. Two sets of parameters are considered, namely error on the SEA model's coefficients, or directly the engineering parameters. The first case is an intrusive approach, but enables to identify the dominant phenomena taking place in a given configuration. The second is non-intrusive and appeals more to engineering considerations, by studying the effect of input parameters such as geometry or material characteristics on the SEA outputs. A study of the distribution of results in each frequency band with the same sampling shows some interesting features, such as bimodal repartitions in some ranges.

Keywords: Sensitivity analysis, uncertainty, SEA, noise reduction,

composite,

1. Introduction

Vibroacoustic design is a topic of great importance in many engineering sectors. Especially in the transportation industries, both on the ground or in aeronautics, noise and vibration have to be addressed in order to achieve competitive products. This has even become more important since a trend towards lightweight design has initiated in order to improve energy efficiency, which has the downside of degrading noise and vibration performance. The wide frequency spectrum which has to be studied leads to different methodologies in handling vibroacoustic problems: some methods deal primarily with low frequencies, and others with high frequencies. Statistical Energy Analysis (SEA) [1] belongs to the second category. It is a widely-used method, which considers average energy quantities through energy balance. SEA modelling is quite simple. The system is divided into simple substructures, and the power balance leads to an algebraic equations giving the total energy stored within each of them. This model requires knowledge of several coefficients, which can be difficult to estimate reliably. For instance, the energy flow balance needs the damping loss factor (DLF) to be provided for each subsystem. The coupling loss factor (CLF) of each couple of subsystems is also needed to close the analytical formulation. CLF and DLF are often provided by a database of materials and interfaces. These quantities can also be estimated experimentally or numerically. The literature about SEA reports a significant amount of publications dealing with SEA inputs estimation in vibroacoustic contexts, either analytically [1] or deriving from

finite element models [2, 3]. The impact of the variability of such inputs on the SEA design can be of great interest at the pre-design stage.

Uncertainty and variability are the core of the SEA approach, as it deals with ensemble statistics rather than deterministic quantities. However, the actual averaging lies in the SEA hypotheses rather than in the mathematical formulation itself, and the account of uncertainty is not explicit in classical SEA. Fahy and Mohammed [4] investigated the effect of uncertainties on the output variance of power flows in SEA systems composed of coupled plates and beams. Work has been done by Langley and Brown [5, 6] to estimate the variance of the kinetic energy of an SEA subsystem. This was extended and validated in [7] for systems with only structural components. Uncertainties in SEA models have been studied by several authors as well: Culla et al. [8] used partial derivative analysis and Design of Experiment (DoE) techniques to study the sensitivity of models to the SEA factors. Partial derivative sensitivity was also used for transfer path analysis by Büssow and Petersson [9]. The effect of the variance of SEA couplig loss factors on transfer path analysis is studied by Aragonès and Guasch [10]. Cicirello and Langley [11] also studied the sensitivity of a mixed FE-SEA model to both parametric and non-parametric uncertainties.Xu et al. [12] proposed two methods to estimate the interval of variability of SEA results for structural-acoustics coupled systems.

The objective of this work is to contribute to the quantification of uncertainty due to model inaccuracy, by establishing a ranking of the most influential parameters of a SEA model. Global sensitivity analysis in general is used to derive indicators of influence for parameters which have broad variation

ranges, as opposed to local methods which target variations around a working point. There are several ways of deriving global indicators [13]. Among these, the class of methods grouped under the term ANOVA (acronym of Analysis of Variance) are based on the variance decomposition [14] as an estimate for the sensitivity of each parameter. The Fourier amplitude sensitivity test (FAST) is one of these methods, which was originally developed by Cukier et al. [15] as a computationally efficient method to compute the ANOVA sensitivity indices, with application in the study of complex chemical reactions. This method has later been reused by Iooss et al. [16] for radiologic risk assessment models. Ouisse et al. [17] applied the FAST method to porous material models, regarding acoustic impedance and absorption. This work was later extended to different models of porous materials with focus on microgeometry in [18]. The parametric approach proposed here can be used both for lack of knowledge of parameters, or for model inaccuracies, and so be used in combination with an interval analysis such as the one proposed by Reynders [19].

SEA models are subject to uncertainty in two forms: lack of knowledge of the input parameters, and modelling errors in evaluating the damping and coupling coefficients. The originality of the present work lies in the application of an ANOVA global sensitivity analysis method to an SEA model in order to identify the contribution of every uncertain parameter to the output variance. Both modelling uncertainties and input parameter variability can be handled in the proposed framework.

The method is first presented on the academic case of noise transmission between two reverberant rooms through a composite plate. Variation on the

coupling coefficients enable to highlight the dominant phenomena occurring in the model. The effect of engineering parameters is then studied on the same academic set-up and an industrial structure. Because the FAST method is a sampling method, the values at samples can also be recovered and used in a statistical analysis enabling to get more information about the distribution, such as the standard deviation or simplified models of the probability law.

This paper is structured as follows: section 2 presents the general SEA model that will be used for the academic case. A brief overview of the FAST sensitivity analysis method is presented in section 3. The uncertainty of modelling itself is investigated on the academic transmission suite case in section 4. Finally, the effect of uncertainties on engineering parameters is studied in section 5 with the same transmission suite example and an industrial test case.

2. SEA modelling

2.1. General SEA equations

SEA modelling is based on the analogy between energy exchanges in vibrating systems and heat transfer between bodies at different temperatures. The mechanical system is decomposed into N elementary subsystems. The power flow between each pair of subsystems is supposed to be proportional to the difference between their total vibrational energies. In addition, each system can dissipate energy, again proportionally to its energy level. The power transferred from subsystem i with total energy E_i to subsystem j with energy E_j in the band centred around frequency f is written

$$P_{ij} = \omega \left(\eta_{ij} E_i - \eta_{ji} E_j \right), \tag{1}$$

where $\omega = 2\pi f$, η_{ij} and η_{ij} are called coupling loss factors (CLF), while the power dissipated in system i is

$$P_{i,diss} = \omega \eta_i E_i, \tag{2}$$

where η_i is the damping loss factor (DLF). All these coefficients depend on the nature of the subsystems and their coupling, as well as on the width of the frequency band considered. The CLFs obey a reciprocity rule, as $\eta_{ij} n_i = \eta_{ji} n_j$ where n_i and n_j are the modal densities of systems i and j. The SEA system is obtained by writing the power balance of each subsystem, where the injected power equates the power losses due to dissipation and couplings:

$$P_{i,inj} = \sum_{j \neq i} P_{ij} + P_{i,diss}. \tag{3}$$

[Figure 1 about here.]

The considered configuration is that of the transmission suite shown on Figure 1, comprising two rooms separated by the studied plate. The plate is made of a sandwich composite material whose core is honeycomb-shaped. The SEA model used in [20] is considered in this study. It consists of 3 subsystems, numbered 1 for the cavity where the source is radiating, 2 for the plate, and 3 for the receiving cavity. The non-resonant transmission introduces a direct coupling between the two rooms, and is taken into account through the CLF η_{13}. The SEA equations then write as a matrix system:

$$\omega \begin{pmatrix} (\eta_1 + \eta_{12} + \eta_{13}) n_1 & -\eta_{21} n_2 & -\eta_{31} n_3 \\ -\eta_{12} n_1 & (\eta_2 + \eta_{21} + \eta_{23}) n_2 & -\eta_{32} n_3 \\ -\eta_{13} n_1 & -\eta_{23} n_2 & (\eta_{31} + \eta_{32} + \eta_3) n_3 \end{pmatrix} \begin{pmatrix} E_1/n_1 \\ E_2/n_2 \\ E_3/n_3 \end{pmatrix} = \begin{pmatrix} P_{inj}^1 \\ 0 \\ 0 \end{pmatrix}, \tag{4}$$

where P_{inj}^1 is the power injected in this frequency band in the source cavity 1.

Since the two rooms are identical and the plate radiates identically on both sides, the following equalities between CLFs, DLFs and modal densities hold, respectively: $\eta_{23} = \eta_{21} = \eta_{rad}$, $\eta_1 = \eta_3 = \eta_{cav}$ and $n_1 = n_3 = n_{cav}$. Since the system is symmetrical, we also have $\eta_{13} = \eta_{31}$. With the reciprocity rule, we also have for all $i, j \in \{1, 2, 3\}$. The energy ratio between the two rooms then writes

$$\frac{E_1}{E_3} = 1 + \frac{2\eta_{rad}\eta_1 n_1 + (\eta_1 n_1 + \eta_{rad} n_2)\eta_2}{\eta_{rad}^2 n_2 + \eta_{13}(2\eta_{rad} + \eta_2)n_1}; \tag{5}$$

The noise reduction index (NR), which is the difference of sound pressure levels in the two rooms, then writes

$$\mathrm{NR} = 10 \log_{10} \left(\frac{E_1}{E_3} \frac{V_3}{V_1} \right), \tag{6}$$

where V_1 and V_3 are the volumes of the two rooms, which are equal in the considered case. The sound transmission loss (TL), defined as the logarithmic ratio of sound intensities on each side of the plate, can be computed from this ratio as well, introducing the receiving cavity's absorption α_{cav}, which is part of the definition of the DLF η_{cav}. According to [20], the TL writes:

$$\mathrm{TL} = 10 \log_{10} \left(\frac{A_2}{S_{cav}\alpha_{cav}} \left(\frac{E_1}{E_3} - 1 \right) \right), \tag{7}$$

where A_2 is the area of the plate and S_{cav} the absorbing surface of the receiving room.

2.2. Evaluation of SEA parameters

2.2.1. Damping loss factors

The damping loss factor for the composite plate can be expressed as a function of frequency f. It is calculated with the following formula [21]:

$$\eta_2 = \eta_{plate} = Af^{-B}. \tag{8}$$

The parameters A and B are found experimentally. The same reference gives $B = 0.63$ as a good fit for experiments on space structures, and coefficient A may vary between 0.1 and 0.6.

The DLF of a room is given from the reverberation time as

$$\eta_{cav} = \frac{2.2}{fT_{cav}}, \tag{9}$$

where $T_{cav} = 0.161\dfrac{V_{cav}}{\alpha_{cav}S_{cav}}$ is the reverberation time and V_{cav} is the volume of the cavity. This equation, known as Sabine's formula, is valid for normal conditions in which the speed of sound in air is $c_0 = 343$ m.s^{-1} and the density of air is $\rho_0 = 1.21$ kg.m^{-3}.

2.2.2. Plate-cavity coupling

The coupling loss factor between the plate and one cavity is linked to the radiation efficiency of the plate, which itself depends on the critical frequency f_c. Maidanik's corrected formulas [22, 23], are used for the radiation resistance of the plate, with following notations: $\tilde{f} = \sqrt{\frac{f}{f_c}}$, $\lambda_c = \frac{c_0}{f_c}$. The plate is rectangular with length l_x and width l_y. The radiation resistance is

then

$$R_{rad} = A_2 \rho_0 c_0 \begin{cases} \sigma_{corner} + \sigma_{edge} & \text{if } f < f_c \\ \sqrt{l_x/\lambda_c} + \sqrt{l_y/\lambda_c} & \text{if } f = f_c \\ \left(1 - \frac{f_c}{f}\right)^{-\frac{1}{2}} & \text{if } f > f_c, \end{cases} \tag{10}$$

where

$$\sigma_{corner} = \begin{cases} 0 & \text{if } f > f_c/2 \\ \dfrac{8c_0^2}{A_2 f_c^2 \pi^4} \dfrac{1 - 2\tilde{f}^2}{\sqrt{\tilde{f}^2(1-\tilde{f}^2)}} & \text{otherwise,} \end{cases} \tag{11}$$

$$\sigma_{edge} = \frac{P_2 c_0}{4\pi^2 f_c A_2} \frac{\left(1 - \tilde{f}^2\right)\left(\ln \frac{1+\tilde{f}}{1-\tilde{f}} + 2\tilde{f}\right)}{\left(1 - \tilde{f}^2\right)^{\frac{3}{2}}}, \tag{12}$$

and $P_2 = 2(l_x + l_y)$ is the perimeter of the plate. The CLF for the power flow from the plate to the cavity is finally:

$$\eta_{rad} = \frac{R_{rad}}{\omega m A_2}, \tag{13}$$

where m is the surface density of the plate and mA_2 is therefore the total mass of the structure.

2.2.3. Non-resonant transmission

The resonant coupling described in the previous paragraph does not take into account non-resonant transmission between the two rooms, also known as mass law. This phenomenon is negligible above the critical frequency, but important below it. It is thus necessary to account for it by introducing a coupling loss factor between the two rooms. This term depends on the room's volume and the mass of the plate. Since the two rooms are identical,

the expression of the CLF is given by [1]:

$$\eta_{13} = \frac{3\rho_0^2 c_0^3 A_2}{2\omega^3 m^2 V_{cav}}; \tag{14}$$

2.2.4. Critical frequency

The critical frequency is the frequency where the wavenumber of free propagating flexural waves k_{bend} is equal to that of a grazing acoustic wave, which reads

$$k_{bend}(f_c) = 2\pi \frac{f_c}{c_0}. \tag{15}$$

This corresponds to the minimum of all possible coincidence frequencies. Since this paper only discusses diffuse fields, by language abuse the terms "coincidence" and "critical frequency" will be used interchangeably. Narayanan and Shanbhag's model [24] for wave propagation in sandwich panels is used, for which the constitutive equation for an isotropic sandwich without damping writes in the frequency domain

$$-D_t k_{bend}^6 - g(D_t + B)k_{bend}^4 - m\omega^2 - \frac{mB}{N}\omega^2 k_{bend}^2 = 0, \tag{16}$$

where $g = 2\frac{G}{Eh_s h_c}$, m is the surface mass of the whole plate, $D_t = \dfrac{Eh_s^3}{6(1-\nu^2)}$ is the skins' bending stiffness, $B = Eh_s(h_c + h_s)^2$ is the overall bending stiffness and $N = Gh_c$ is the shear stiffness. In these definitions, E is the Young's modulus of the skins, G the shear modulus of the core, h_c and h_s respectively the thickness of the core and each skin, and ν is the Poisson's ratio of the skins. Combining Eq. (16) with Eq. (15), gives the equation to which the critical frequency is solution

$$D_t \left(2\pi \frac{f_c}{c_0}\right)^4 + \left(\frac{g(D_t + B)}{c_0^2} + \frac{mB}{N}\right)(2\pi f_c)^2 w + mc_0^2 = 0. \tag{17}$$

As this equation is a second order polynomial in f_c^2, the positive root is the critical frequency.

2.2.5. Modal densities

The modal density of a rectangular acoustic cavity surrounded by hard walls is classically evaluated with the following formula [20]

$$n_{cav} = \frac{4\pi f^2 V_{cav}}{c_0^3} + \frac{\pi f S_{cav}}{2c_0^2} + \frac{P_{cav}}{8c_0} \tag{18}$$

where V_{cav}, S_{cav} and P_{cav} are respectively the volume, surface and perimeter of the cavity. The perimeter P_{cav} is the sum of the lengths of the cavity's edges, and is independent of the plate.

The modal density of a composite plate is obtained from the wave propagation analysis of the plate

$$n_2 = A_2 k_{bend} \frac{\mathrm{d}k_{bend}}{\mathrm{d}\omega}, \tag{19}$$

where the expression for k_{bend} with respect to frequency is obtained again from Eq. (16). All the expressions of the SEA coefficients are averaged over third-octave frequency bands when used in Eq. (5).

3. The FAST method

3.1. Analysis of variance

One parameter's influence on the model output can be quantified by the impact it has on the variance in the given design range. In the following development, a generic mathematical model is considered. A model is a real

valued function f defined over K^n, where $K = [0, 1]$. With appropriate scaling and translations, any model defined over continuous ranges of parameters can be represented that way.

For a given model f linking input parameters $\mathbf{x} = (x_1, ...x_n)$ to a scalar output $y = f(\mathbf{x})$, the Hoeffding decomposition, or high order model representation (HDMR) [14], writes:

$$y = f(x_1, x_2, ...x_n) = f_0 + \sum_{i=1}^{n} f_i(x_i) + \sum_{i<j} f_{ij}(x_i, x_j) + ... + f_{1...n}(x_1, ..., x_n). \tag{20}$$

There exist a unique such decomposition so that every function f_U involved in the decomposition, except f_0, has zero mean over its range of variation $K|_U$, which is the subspace of K spanned by the dimensions contained in subset U, or in mathematical terms,

$$\text{for all } U \subset [1, n], \quad \int_{K|_U} f_U(x_U) \mathrm{d}x_U = 0. \tag{21}$$

For a given set of indices $U \subset [1, n]$, the partial variance is therefore the variance of f_U

$$V_U = \int_{K|_U} f_U(x_U)^2 \mathrm{d}x_U. \tag{22}$$

The sensitivity index relative to the set U is expressed as the ratio of the variance of the function f_U to the total variance of the model:

$$\mathrm{SI}(U) = \frac{V_U}{V}. \tag{23}$$

The computation of all the 2^n sensitivity indices is needed to represent completely the model, however this becomes quickly a very costly task in terms of computational time, as they have to be evaluated by numerical

integration. However, most information about a parameter's influence can be found in the first-order sensitivity index and the total sensitivity index, which can be computed more efficiently with the FAST method.

For a given parameter $i \in [1, n]$, the main effect (ME) is then the sensitivity index relative to the 1-dimensional function f_i:

$$\mathrm{ME}(i) = \mathrm{SI}(\{i\}).$$

Another interesting sensitivity measure for a given parameter i is the total sensitivity index, defined as the sum of the indices of all sets of parameters U to which i belongs:

$$\mathrm{TSI}(i) = \sum_{\substack{U \subset [1,n] \\ i \in U}} \mathrm{SI}(U). \tag{24}$$

3.2. Main effect computation

The functions f_U are defined recursively [14], and their explicit computation, as well as the computation of their variances, demands a high number of integrals on subsets of parameter space K. The principle behind the FAST method is to avoid the evaluation of these multidimensional integrals by a clever sampling of K. This sampling is made along a space filling curve, which is periodic with different periods in each dimension of K, allowing for Fourier analysis. We use here the sampling function proposed by Saltelli et al. [25], defining the following parametric curve:

$$x_i(s) = \frac{1}{2} + \frac{1}{\pi} \arcsin\left(\sin\left(\omega_i s + \varphi_i\right)\right), \tag{25}$$

where the integers ω_i are chosen according to [15]. Their values are recalled for 4 and 5 parameters in Table 1. The values φ_i are real numbers randomly

chosen in the interval $[0; 2\pi]$. This allows to average the results over several analysis made with different values of φ_i in order to better span the parameter space K.

[Table 1 about here.]

The function $s \mapsto (x_1(s), ..., x_n(s))$ is 2π-periodic. The number of samples is $N >> 2\omega_n + 1$, taken in the $[0, 2\pi]$ interval for the variable s. Let the model output be denoted $y_k = f(\mathbf{x}_k)$, where $\mathbf{x}_k = (x_1(s_k), ..., x_n(s_k))$. The discrete Fourier transform $\hat{y}_k$ of the vector of the y_k can be easily computed numerically.

The total variance of the function in the design space is computed with Parseval's theorem as

$$V = \int_K \left(f^2(x) - f_0^2\right) \mathrm{d}x \approx \sum_{k=1}^{N} y_k^2 = \sum_{k=1}^{N} \hat{y}_k^2 \tag{26}$$

The contribution of parameter i will then be:

$$V_i = \sum_{k=1}^{M} \hat{y}_{k\omega_i}^2, \tag{27}$$

leading to the first-order sensitivity indices $\mathrm{ME}(i) = \frac{V_i}{V}$.

3.3. Total sensitivity index computation

A method proposed in [25] is to assign one rather high integer frequency ω_i to parameter i and a set of low frequencies $\{\omega_{\sim i}\}$ to all other parameters. The same sampling curve as defined in Eq. (25) is used with these frequencies, and post-processed so that the lowest order harmonics give the partial variance

$D_{\sim i}$ relative to all parameters but i. The total sensitivity index of parameter i is then

$$TSI(i) = 1 - \frac{V_{\sim i}}{V}. \tag{28}$$

3.4. Interpretation

By definition, the sensitivity indices range between 0 and 1. The sum of main effects is less than or equal to 1. The difference $1 - \sum_{i=1}^{n} \mathrm{ME}(i)$ is a measure of how much interaction there is between parameters to produce the variance, i.e. how much of the variance cannot be explained by variations of each parameter individually. This difference is exactly zero only for models whose outputs can be expressed as a sum of one-variable functions of the inputs. These models are also called additive models. For such models, main effect and total sensitivity indices are equal.

The first-order index represents the share of the output variance that is explained by the considered parameter alone. Most important parameters therefore have high ME, but a low ME does not mean the parameter has no influence, as it can be involved in interactions.

The total index is a measure of the share of the variance that is removed from the total variance when the considered parameter is fixed to its reference value. Therefore parameters with low TSI can be considered as non-influential.

4. Model uncertainty

The formulas established in the previous sections are approximations, especially in the case of Maidanik's formulas, which were primarily established for a thin plate. As the behaviour of a sandwich structure implies some

shear in the core that is not taken into account, it is expected that the SEA parameters calculated above contain some inaccuracy. Other error-prone parameters include the DLFs, as damping is notoriously difficult to evaluate for complex structures.

The sensitivity of the NR with respect to uncertainties in the following four SEA parameters is studied with the FAST method: the plate-cavity CLF η_{rad}, the cavity absorption α_{cav}, the plate DLF η_{plate}, and the critical frequency f_c. The academic design chosen has following characteristics: the cavities are cubic with an edge length of 5.1m, the size of the plate is 0.8m$\times$1.2m. The plate is made of a composite sandwich with isotropic core (shear modulus G=400MPa, thickness h_c=12.7mm) and isotropic skins (Young modulus E=50GPa, Poisson ratio ν=0.1, thickness h_s=1mm). The overall surface density of the plate is $m = 5\text{kg.m}^{-2}$. The fluid is air with density $\rho_0 = 1.21\text{kg.m}^{-3}$ and sound speed $c_0 = 343\text{m.s}^{-1}$. Under these conditions, the critical frequency is around 640Hz.

In order to study this uncertainty, the reference values of each parameter are evaluated for each frequency band with the formulas described in section 2. The reference value of parameter i is then multiplied by a random error factor $\varepsilon(i)$ with a probability law centred on 1. For example, if the reference DLF in the plate is denoted η_{plate}, then the error factor is denoted $\varepsilon\left(\eta_{plate}\right)$, which should not be interpreted as a function of η_{plate}, but simply as a writing commodity. The actual DLF in one sample is then $\eta_{plate}\varepsilon\left(\eta_{plate}\right)$.

Two kinds of probability laws are considered for the error factors, namely a uniform law, in which the possible values are bounded and equiprobable, and a lognormal law, which only restricts the error factor to positive values,

with an average value equal to 1.

4.1. FAST results

4.1.1. Uniform law on uncertainty parameters

The uniform laws are chosen to be centred on 1, and with non-negative values. The chosen bounds for each parameter are presented in Table 2. The error on the critical frequency is chosen rather low ($\pm 10\%$), while that on the plate's internal damping is very high ($\pm 40\%$).

[Table 2 about here.]

Figure 2 shows the first-order sensitivity indices (ME) of all the considered parameters for the NR in each third-octave band between 100Hz and 20kHz. It can be seen that the CLF between the plate and the cavities is dominant over most of the frequency range, except in the bands around 800Hz, where the nominal value of the critical frequency lies, and in which the error on f_c is dominant. This can be expected, as all energy flowing between the emitting and receiving cavities has to go through the plate, no indirect coupling being taken into account in this model. Despite its high uncertainty ($\pm 40\%$), the plate's damping is on the contrary relatively unimportant on the whole range, meaning that whatever its value in the considered range, much less power is dissipated in the plate than transferred to the receiving cavity. The effect of the critical frequency is limited to the third octave bands around coincidence, and negligible for extreme high and low frequencies.

The asymmetry observed between high and low frequencies is partly due to the logarithmic scale used but also mainly to the expression of the radiation efficiency (Eq. (10)), which tends to infinity when f approaches f_c as

$\left|1-\frac{f}{f_c}\right|^{-\frac{3}{2}}$ when $f < f_c$, faster than $\left|1-\frac{f}{f_c}\right|^{-\frac{1}{2}}$ when $f > f_c$. As the NR varies with η_{rad}^{-1}, this means that an error on f_c will have more importance when $f < f_c$ than when $f > f_c$.

It can be noted that the sum of the main effects is always close to 1, meaning that the model is free from interactions between parameters in the case a uniform law is used for all of them.

[Figure 2 about here.]

4.1.2. Lognormal law

A lognormal law is traditionally characterised by the mean μ and the standard deviation σ of the associated Gaussian law, while its actual average is

$$\mu_l = \exp\left(\mu + \frac{\sigma^2}{2}\right), \tag{29}$$

and its actual standard deviation is

$$\sigma_l = \left(\exp(\sigma^2) - 1\right)\exp(2\mu + \sigma^2). \tag{30}$$

The parameters of the lognormal law presented in Table 3 are chosen so that their actual mean is 1, and their actual standard deviations match those of the corresponding uniform laws.

[Figure 3 about here.]

[Table 3 about here.]

The main effects from the FAST analysis of the NR in this case are presented on Figure 4. They compare well with those computed in the previous

section with a uniform law, except the fact that they do not add up to 1, but to a slightly lower value around 0.95, indicating the presence of interactions. As the parameters vary in a broader range, albeit with a low probability, this indicates that the model is not fully additive in this case, and that the use of a non-uniform probability law induces some interaction between parameters

[Figure 4 about here.]

4.2. Statistical considerations

With the sampling used for the FAST analysis, it is possible to compute some statistical features of the response, which are summarized on Figure 5 for the uniform law and Figure 6 for the lognormal law. These two figures present the distribution of the response on a coloured scale, the bluer part indicating the least probable values, and the redder the most probable. The mean and the interval width of ± 1 standard deviation around the mean are superimposed as black and dashed black lines respectively, and the nominal response is shown as a dashed purple line.

It can be seen that in both cases, for most of the frequency range the nominal response coincides with the average, but the most probable response may differ by several dB, especially in the coincidence range around 800Hz. The lognormal law show as expected a wider range: as the parameter values are theoretically unbounded, so is the response. The standard deviation is nearly the same in both cases, and reaches about 2dB, which is acceptable for most industrial applications. The considered errors on modelling parameters are therefore reasonable here.

[Figure 5 about here.]

[Figure 6 about here.]

5. Parametric uncertainty

One of the main aims of sensitivity analysis is to study the effect of input parameters. While the analysis in section 4 was focused on internal parameters of the SEA model, we propose here to apply it to parameters that are more readily manipulable by a designer, namely material parameters. The two cases considered are first the same academic transmission suite, and second a test structure shaped like a mock-up of a space structure.

5.1. Transmission suite

The plate between the two rooms of the transmission suite being made of sandwich composite material, the most relevant parameters from an engineering point of view are the Young's modulus of the skins E, the equivalent transverse shear modulus of the core G, the overall surface mass m, the plate's damping η_{plate} and the cavity's absorption coefficient α_{cav}. The damping loss factor is calculated with the formula defined in Eq. (8). The uncertainty is applied on the coefficient A, while the exponent B is constant and taken equal to 0.63, which is thus equivalent to the uncertainty studied previously.

[Table 4 about here.]

The main effects on the NR are presented in Figure 7. It is noticeable that the absorption of the cavity has a high impact, accounting for between 50 and 60% of the variance everywhere, except around coincidence. The second most important parameter is mass below coincidence, and the shear modulus above it.

[Figure 7 about here.]

The same analysis on the transmission loss (TL) defined in Eq. (7), which should neutralise the effect of absorption in the rooms exhibits a similar ranking of parameters, except that absorption does no longer play a role, as shown in Figure 8.

[Figure 8 about here.]

These results are consistent with a previous study made on an analytical model of the same configuration [26]: mass is dominant in low frequencies, while the influence of stiffness peaks around coincidence, and the effects of shear and damping are predominant in high frequencies. Both for NR and TL, the model is additive for all frequency ranges, except the coincidence range, where a high level of interaction is observed. This is due to the expression of the critical frequency as a function of mass and stiffness of the plate: the value of the critical frequency has more effect on the overall variability than the drop in TL that occurs at this frequency.

5.2. Industrial structure

The same kind of analysis was finally applied to a structure composed of two cones and a cylinder, as shown in Figure 9a. It will be referred to as SYLDA-like, because its configuration is loosely inspired from the Ariane 5 SYLDA double launch system. The holes on the top and bottom sides are supposed to be hermetically sealed. An SEA model has been implemented in an industrial code, based on modal formulations for the CLFs. Five subsystems are considered, one cavity representing the exterior diffuse sound field, the inner cavity, and three structural parts: the top and bottom conical shells

and the cylindrical shell in the middle, as shown in Figure 9b. All shells are made in the same sandwich material, and feature the same engineering parameters as the plate in the previous subsection (Table 4). The outer cavity is open, and the sound field is supposed to be uniform and diffuse in the vicinity of the shell. The model output is the noise reduction (NR) factor, which is the difference in sound pressure levels between the outer and inner cavities.

[Figure 9 about here.]

Figure 10 shows the results of the FAST analysis by third-octave bands between 400Hz and 16 kHz. The lowest frequency band is chosen because there are no structural modes in the lower (320Hz) third-octave band, making the mode-based model used unable to compute CLFs in this range. The main effects (ME) presented in 10a indicate an additive model except again in the coincidence range. This time, as the transmission occurs through the whole surface of the structure, the cavity absorption is again predominant in most of the frequency range, while the effect of mass is sensible only in low frequencies, and the effect of shear increases with frequency. The total sensitivity indices (TSI) presented in 10b are, as expected from the previous figure, identical to the ME except in the band where most critical frequencies appear, where the highest TSIs are those of the mass and Young's modulus, indicating again that the variance of the NR in this band is largely due to an interaction between these two factors, which determine the value of the critical frequency.

[Figure 10 about here.]

The FAST sampling here leads to interesting considerations concerning the distribution of the response (Figure 11): in this case, the average response is globally centred in the distribution for all third-octave-bands, except the one centred on 630Hz, which contains the reference critical frequency. In this octave the probability density function is not centred, but exhibits two local maxima, one being a real maximum around 4dB, 2dB lower than the average, and one around 8dB, more than one standard deviation away from the average, which pleads in favour of looking for more advanced statistical features of the response distribution than just the mean.

[Figure 11 about here.]

6. Conclusion

The parametric sensitivity analysis method FAST has been employed in this paper to study the effect of model and parametric uncertainties on the noise reduction and transmission loss through composite structures modelled with SEA. The academic case of a transmission suite allowed us to apply uncertainties on several SEA model features such as coupling loss factors and damping loss factors, showing that the most important parameters are, unsurprisingly, the plate-cavity coupling and, much less, the cavity's absorption coefficient. The effect of the probability law was also tested, comparing a uniform law on the model error parameters to a lognormal law. Both results were found compatible, as the laws were chosen to have the same average and standard deviation, but the unboundedness of the parameter range with the lognormal law leads to interactions between parameters. Concerning uncertainties on design or engineering parameters, the results found on

the academic case are consistent with common knowledge, while the more general frame of the SEA method allowed us to validate these results on a more complex industrial-like case. It should be noted that the results in this case are very specific to the chosen set-up, and hence cannot be intuitively extrapolated from the results of the academic case.

The fact that the FAST method uses a sampling of the parameter space makes it possible to derive some informations about the general statistics of the response. For the studied cases, the most probable response is usually close to the nominal and to the average response, but difference may arise especially around the critical frequency, when the interactions between parameters in the sense of ANOVA is high.

7. Acknowledgements

The authors would like to gratefully acknowledge Airbus Defence and Space for their financial support. This project is part of the international cooperation project CRIAQ ACOU504_INTL.

References

[1] R. H. Lyon, R. G. DeJong, Theory and application of Statistical Energy Analysis, Butterworth-Heinemann, 1995.

[2] N. Totaro, C. Dodard, J. L. Guyader, SEA Coupling Loss Factors of Complex Vibro-Acoustic Systems, ASME Journal of Vibration and Acoustics 131 (4) (2009) 8 pages.

[3] A. Thite, B. Mace, Robust estimation of coupling loss factors from finite element analysis, Journal of Sound and Vibration 303 (3–5) (2007) 814 – 831.

[4] F. Fahy, A. Mohammed, A study of uncertainty in applications of SEA to coupled beam and plate systems, part I: Computational experiments, Journal of Sound and Vibration 158 (1) (1992) 45 – 67.

[5] R. S. Langley, A. W. M. Brown, The ensemble statistics of the band-averaged energy of a random system, Journal of Sound and Vibration 275 (2004) 847–857.

[6] R. S. Langley, A. W. M. Brown, The ensemble statistics of the energy of a random system subjected to harmonic excitation, Journal of Sound and Vibration 275 (2004) 823–846.

[7] V. Cotoni, R. Langley, M. Kidner, Numerical and experimental validation of variance prediction in the statistical energy analysis of built-up systems, Journal of Sound and Vibration 288 (3) (2005) 701 – 728.

[8] A. Culla, W. D'Ambrogio, A. Fregolent, Parametric approaches for uncertinty propagation in SEA, Mechanical Systems and Signal Processing 25 (2011) 193–204.

[9] R. Büssow, B. A. T. Petersson, Path sensitivity and uncertainty propagation in SEA, Journal of Sound and Virbation 300 (2007) 479–489.

[10] A. Aragonès, O. Guasch, Ranking paths in statistical energy analysis models with non-deterministic loss factors, Mechanical Systems and Signal Processing 52–53 (2015) 741 – 753.

[11] A. Cicirello, R. S. Langley, The vibro-acoustic analysis of built-up systems using a hybrid method with parametric and non-parametric uncertainties, Journal of Sound and Vibration 332 (9) (2013) 2165 – 2178.

[12] M. Xu, Z. Qiu, X. Wang, Uncertainty propagation in SEA for structural-acoustic coupled systems with non-deterministic parameters, Journal of Sound and Vibration 333 (2014) 3949–3965.

[13] A. Saltelli, M. Ratto, T. Andres, F. Campolongo, J. Cariboni, D. Gatelli, M. Saisana, S. Tarantola, Global Sensitivity Analysis: The Primer, John Wiley & Sons, 2008.

[14] I. M. Sobol, Sensitivity analysis for nonlinear mathematical models, Mathematical modeling and computational experiment 1 (1993) 407–414.

[15] R. I. Cukier, C. M. Fortuin, K. E. Shuler, A. G. Petschek, J. H. Schaibly, Study of the sensitivity of coupled reaction systems to uncertainties on rate coefficients. I. Theory, Journal of Chemical Physics 59 (8).

[16] B. Iooss, F. Van Dorpe, N. Devictor, Response surfaces and sensitivity analyses for an environmental model of dose calculations, Reliability Engineering and System Safety 91 (10–11) (2006) 1241–1251, the Fourth International Conference on Sensitivity Analysis of Model Output (SAMO 2004).

[17] M. Ouisse, M. Ichchou, S. Chedly, M. Collet, On the sensitivity analysis of porous material models, Journal of Sound and Vibration 331 (2012) 5292–5308.

[18] O. Doutres, M. Ouisse, N. Atalla, M. N. Ichchou, Impact of the irregular microgeometry of polyurethane foam on the macroscopic acoustic behavior predicted by a unit-cell model, The Journal of the Acoustical Society of America 136 (4) (2014) 1666 – 1681.

[19] E. Reynders, Parametric uncertainty quantification of sound insulation values, Journal of the Acoustical Society of America 135 (2014) 1907–1918.

[20] R. Zhou, M. J. Crocker, Sound transmission loss of foam-filled honeycomb sandwich panels using statistical energy analysis and theoretical and measured dynamic properties, Journal of Sound and Vibration 329 (2010) 673–686.

[21] B. Troclet, Prediction of the vibroacoustic response of the Ariane 4 fairing and the equipment bay, in: G. C. Maling, Jr. (Ed.), Inter-Noise 89 - Engineering for Environmental Noise Control, 263–266, 1989.

[22] G. Maidanik, Response of ribbed panels to reverberant acoustic fields, Journal of the Acoustical Society of America 34 (1962) 809–826.

[23] M. J. Crocker, A. J. Price, Sound transmission using statistical energy analysis, Journal of Sound and Vibration 9 (1969) 469–486.

[24] S. Narayanan, R. L. Shanbhag, Sound transmission through a damped sandwich panel, Journal of Sound and Vibration 80 (3) (1982) 315–327.

[25] A. Saltelli, S. Tarantola, K. P. S. Chan, A quantitative model-independent method for global sensitivity analysis of model output, Technometrics 41 (1) (1999) 39–56.

[26] J.-L. Christen, M. Ichchou, B. Troclet, O. Bareille, M. Ouisse, Global sensitivity analysis of analytical vibroacoustic transmission models, Journal of Sound and Vibration 368 (2016) 121 – 134.

List of Figures

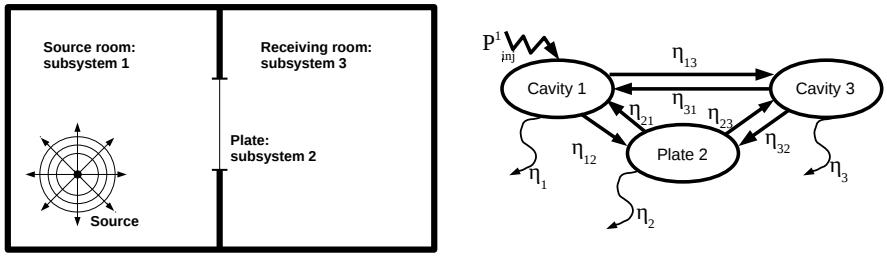

Figure 1: Schematic of a transmission suite and its SEA model

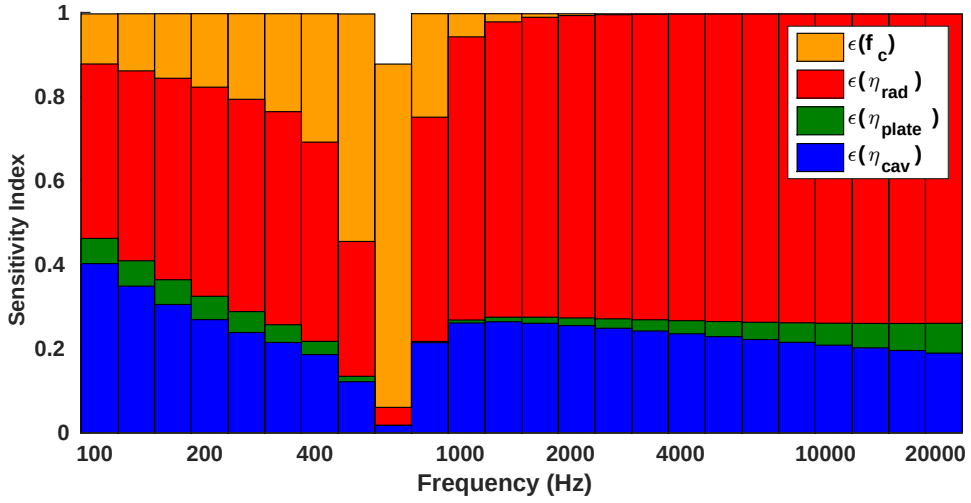

Figure 2: Sensitivity indices of the NR for model error parameters with uniform law (for each bar, from top to bottom: f_c, η_{rad}, η_{plate}, α_{cav})

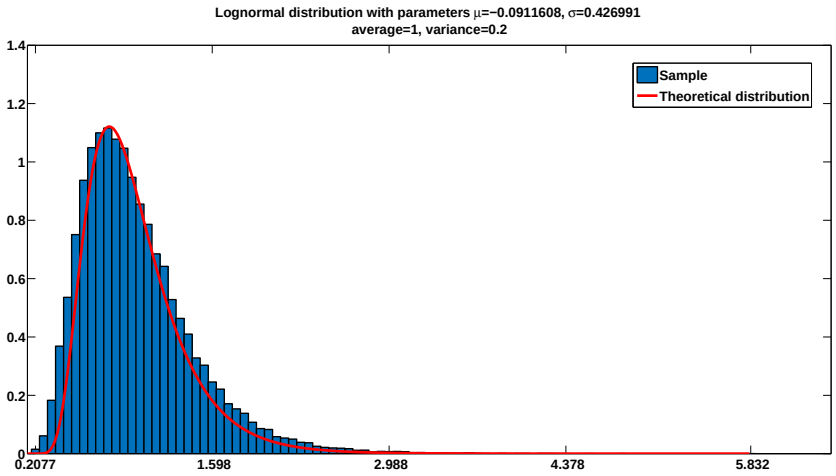

Figure 3: Probability density function of a lognormal law and distribution of a random sample

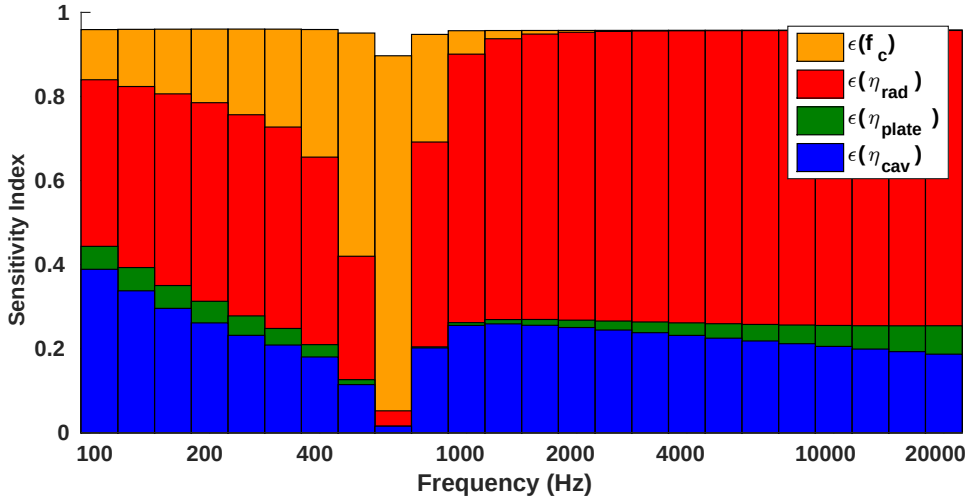

Figure 4: Sensitivity indices of the NR for model error parameters with lognormal law (for each bar, from top to bottom: f_c, η_{rad}, η_{plate}, α_{cav})

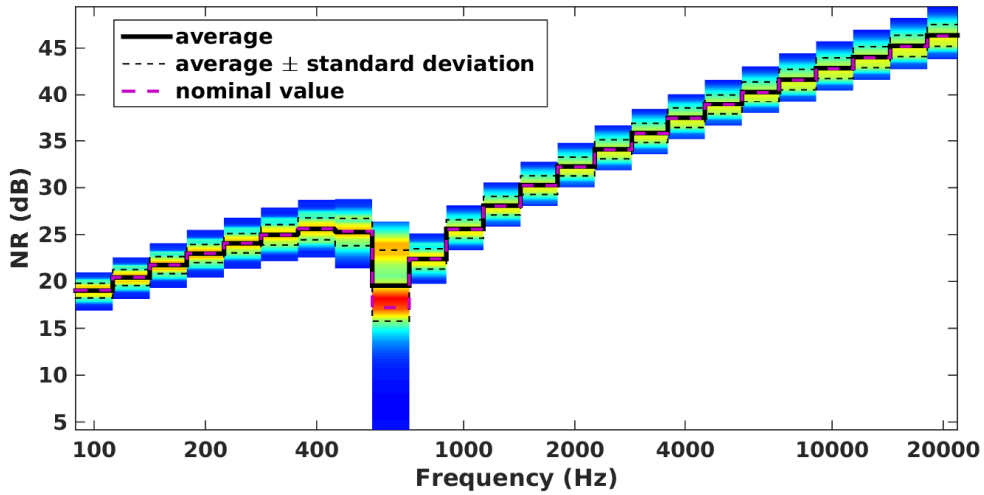

Figure 5: Distribution of the NR around the mean for the "model error" setting and uniform distributions

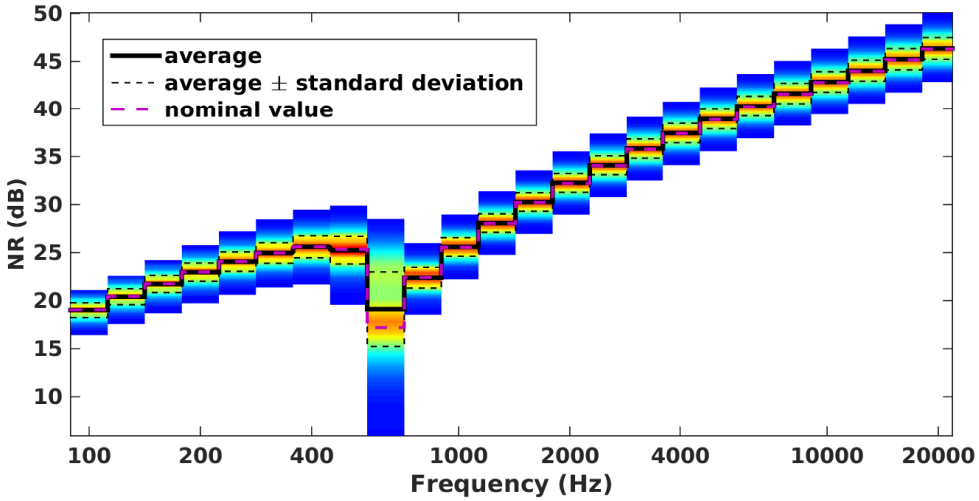

Figure 6: Distribution of the NR around the mean for the "model error" setting and lognormal distributions

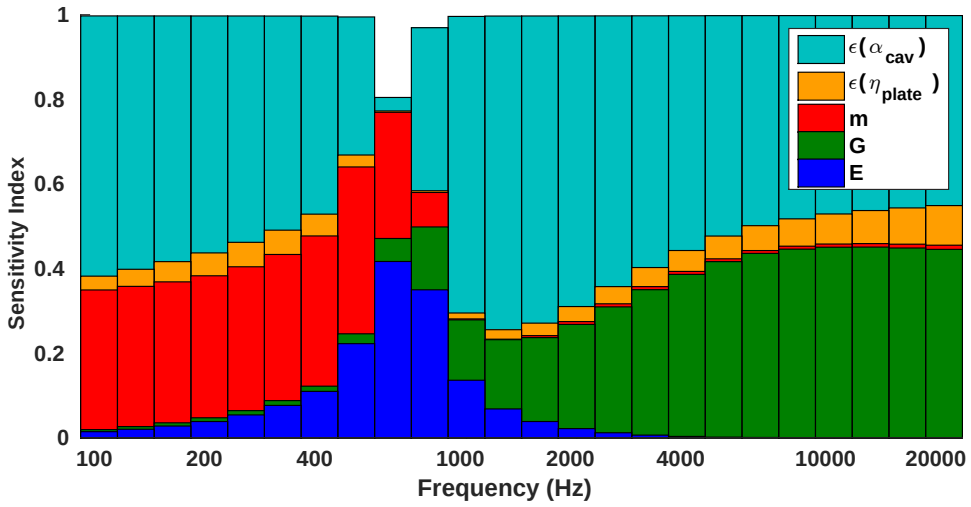

Figure 7: Sensitivity indices of engineering parameters for the NR of the transmission suite. For each bar, from top to bottom: α_{cav}, η_{plate}, m, G, E.

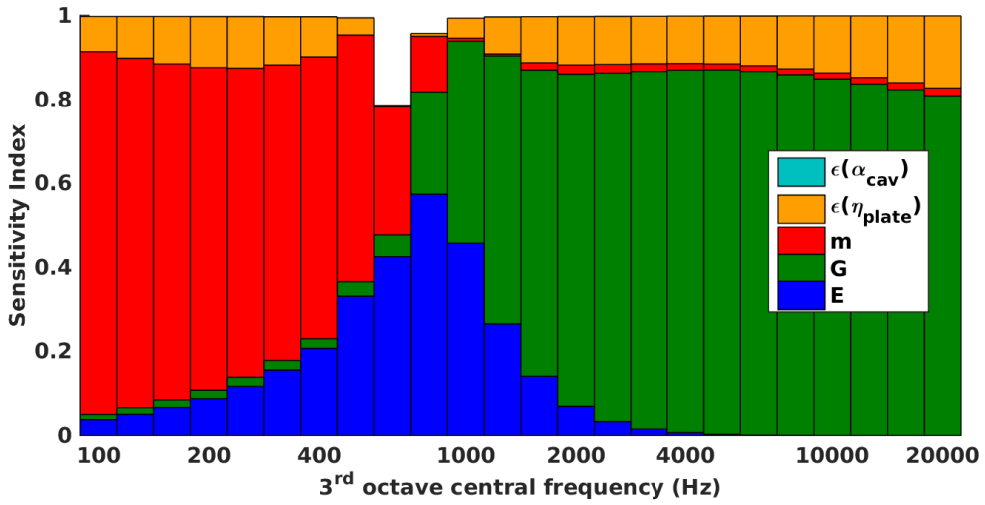

Figure 8: Sensitivity indices of engineering parameters for TL of the transmission suite. For each bar, from top to bottom: α_{cav} (too small to be visible), η_{plate}, m, G, E.

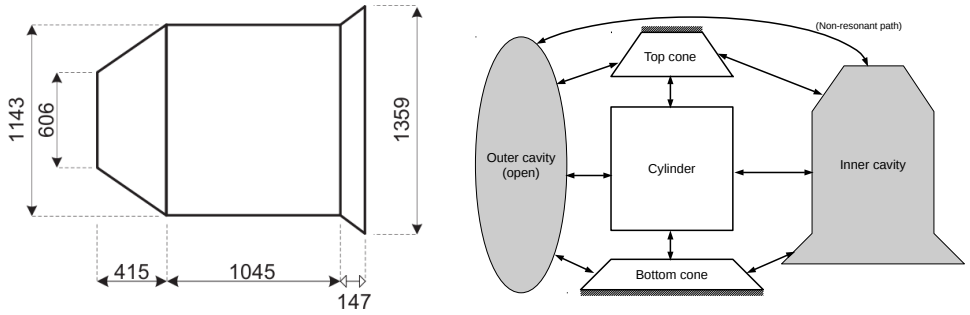

(a) Dimensions in mm.

(b) SEA subsystems and connections

Figure 9: SEA model of the SYLDA-like structure.

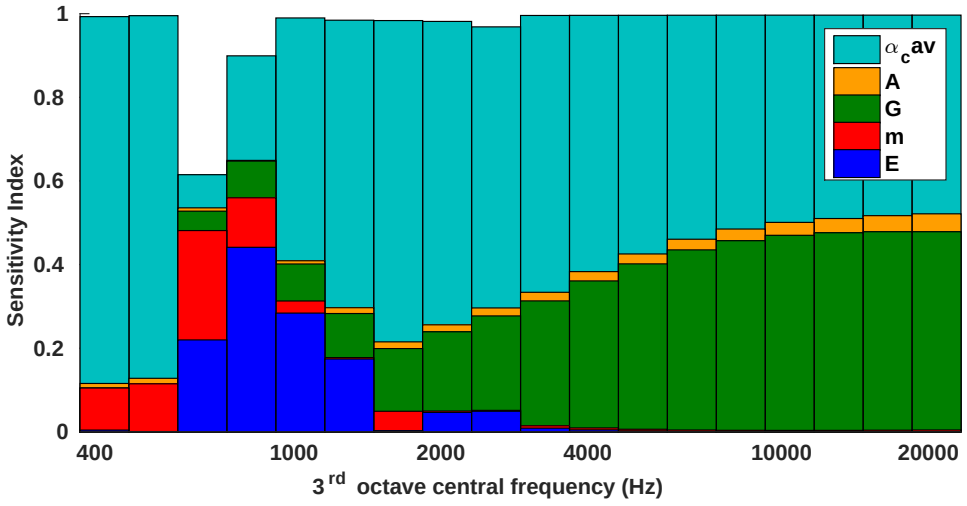

(a)

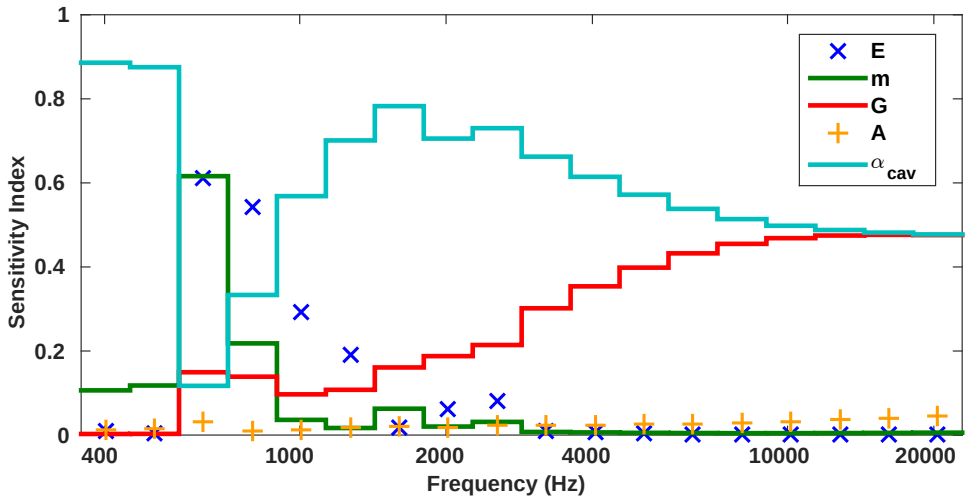

(b)

Figure 10: Main effect (10a) and Total Sensitivity indices (10b) of the five engineering parameters of the SYLDA-like structure

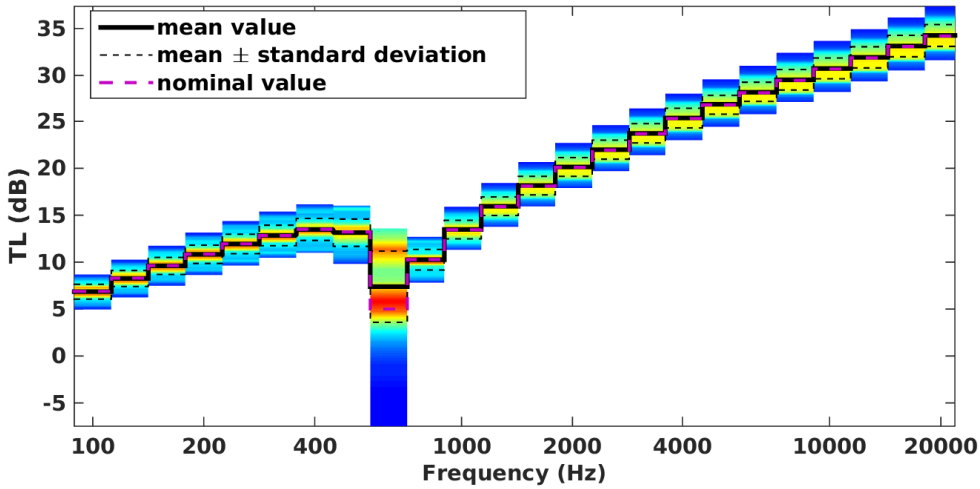

Figure 11: Distribution of the NR around the mean for SYLDA-like test case.

List of Tables

Number of parameters	Frequencies
4	[11; 21; 27; 35]
5	[11; 21; 27; 35; 39]

Table 1: Integer frequencies for the FAST method for 4 and 5 parameters.

Name	Description	Uncertainty
f_c	Critical frequency	$\pm 10\%$
η_{rad}	Plate-cavity CLF	$\pm 30\%$
η_{plate}	Plate damping parameter	$\pm 40\%$
α_{cav}	Cavity absorption	$\pm 20\%$

Table 2: Parameters of the uniform laws used for the model uncertainty parameters

Name	Description	Standard deviation
f_c	Critical frequency	0.0577
η_{rad}	Core shear modulus	0.1732
η_{plate}	Plate damping parameter	0.2309
α_{cav}	Cavity absorption	0.1155

Table 3: Actual standard deviations σ_l of the lognormal laws used for the model uncertainty parameters. The mean μ_l is always equal to 1.

Name	Description	Unit	Reference value	Uncertainty
E	Skin Young modulus	GPa	50	$\pm$15 %
m	Surface density	kg.m^{-2}	5.0	$\pm$10%
G	Core shear modulus	GPa	0.24	v30%
η	Plate damping	–	0.6	$\pm$30%
α_{cav}	Cavity absorption	–	0.1	$\pm$30%

Table 4: Parameters of the uniform laws used for the engineering parameters